ALLEGRO ECAL cross-talk emulation and measurement of the Higgs boson width at FCC-ee

Zhibo Wu, Hind Taibi, Marco Delmastro, Olivier Arnaez

08/10/2024

ALLEGRO detector concept

- A general purpose detector for FCC-ee (√s=90-360 GeV): A Lepton coLider Experiment with Granular calorimetry Read-Out.
- Key feature: High granularity noble liquid EM calorimeter (ECAL).
  - ➢ LAr or LKr with Pb or W.
  - ➢ Multi-layer PCB as read-out electrode.
  - ➢ ECAL inside the 2 T solenoid sharing the cryostat.
- Other sub-detector systems: vertex detector, drift chamber, HCAL and muon tagger.
- Designed for full FCC-ee physics program and focused on particle identification (with the help of particle flow).

Layout of ALLEGRO

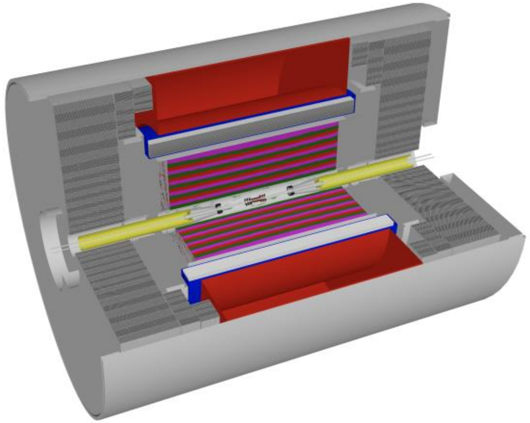

3D-view of ALLEGRO

ECAL barrel

The design of the barrel region ECAL is based on the ATLAS LAr ECAL, but adapted to lepton collider experiment.

- 10 times higher granularity.
- New electrode geometry: straight read-out electrode with 50-degree inclination angle.

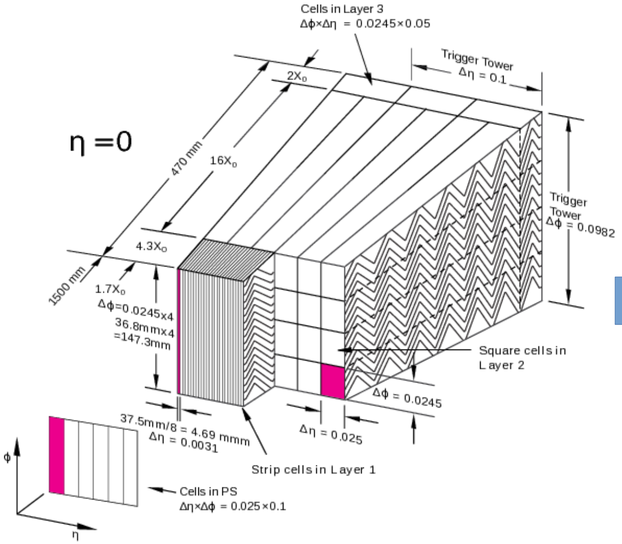

The accordion-like ECAL of ATLAS

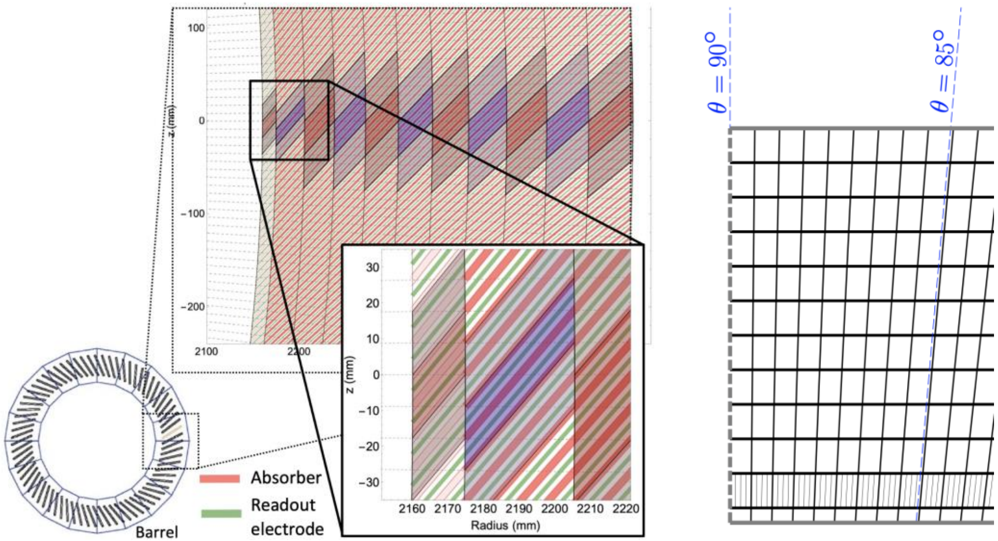

ALLEGRO ECAL with high granularity

Read-out electrode structure

- Printed circuit board technology allows high granularity.
- Various couplings between calorimeter cells and signal traces inside the read-out electrode generate cross-talk → Need for shielding.

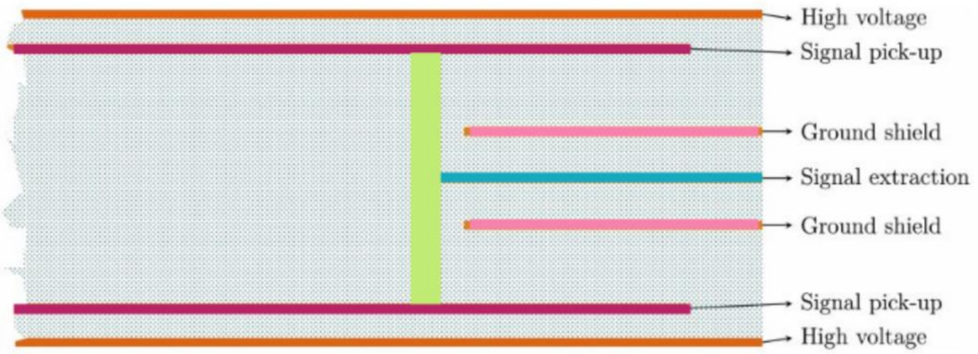

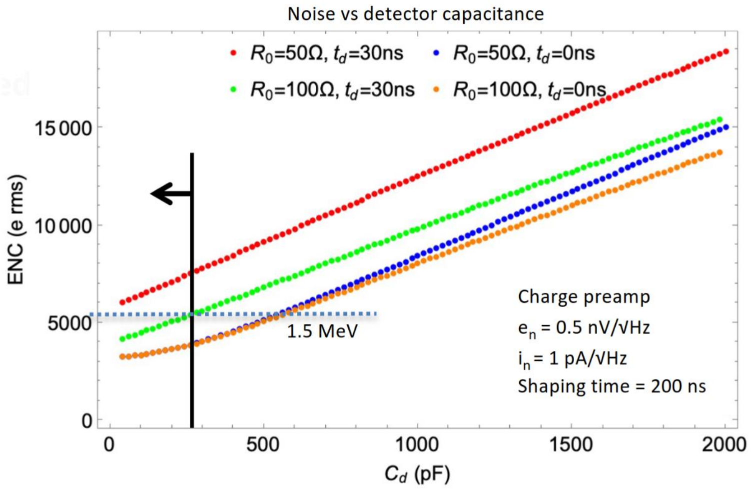

Side view of the 7-layer PCB for the read-out electrode.
Larger shielding suppresses cross-talk but increases electronic noise.

Measurement of electrode cross-talk

- Electrical properties of the electrode is measurement in the lab.
- Cross-talk impact on signal amplitude is reduced when the ionisation signal is processed by shaping filter. Longer shaping time results in smaller effect.

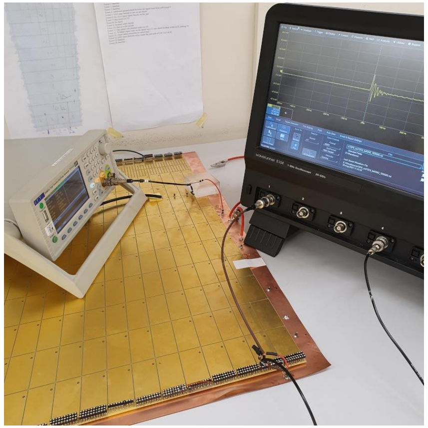

Lab setup:
(a) 300 ns wide 1 V peak is injected to the electrode at 5 ms intervals.
(b) Signals are read from the oscilloscope.

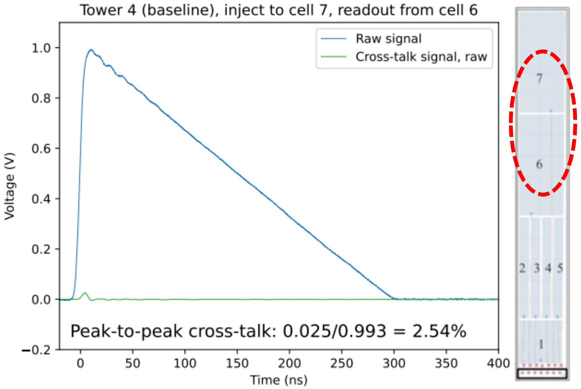

The shark-fin signal appears on the electrode receiving the injection, as well as the cross-talk on a radial neighbour.

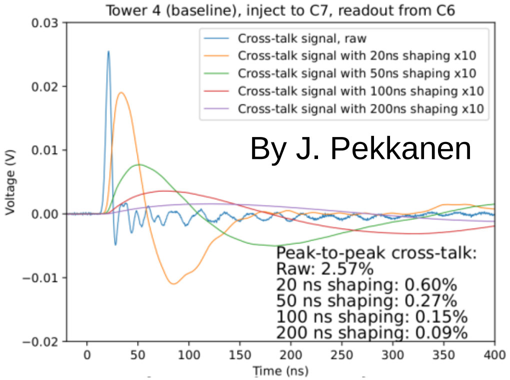

Cross-talk can be efficiently reduced by introducing a pulse shaping (e.g. ATLAS-like RC-CR2 shaper) and choosing a long shaping time (e.g. 200 ns).

Cross-talk emulation in the FullSim

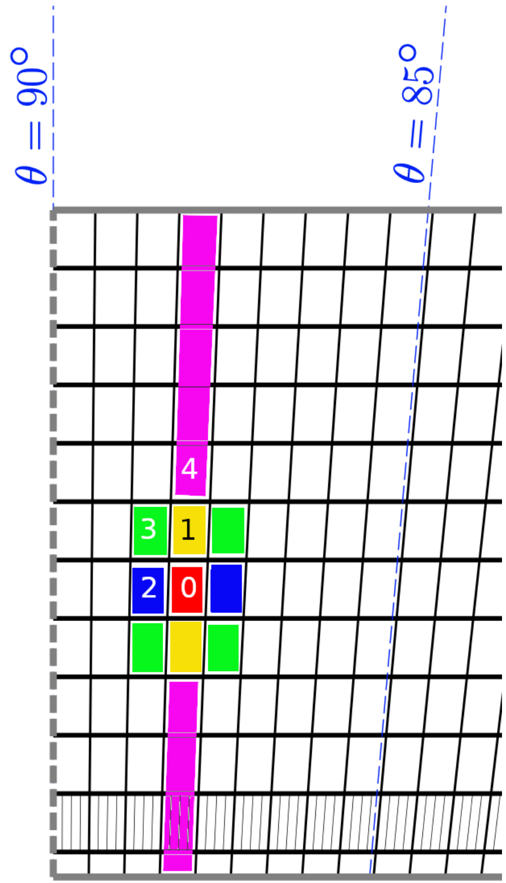

Schematic drawing of CERN prototype PCB

- The emulation of electrode cross-talk has been implemented in the full simulation for ALLEGRO (handled in reconstruction).
- 4 types of cross-talk neighbours are considered in the emulation.

Type	1: Radial	2: Theta	3: Diagonal	4: Tower
Crosstalk	0.7%	0.3%	0.04%	0.1%

Crosstalk coefficients are taken from the measurement on CERN prototype PCB, with a pulse shaping of 50 ns.
No inner/outer radial asymmetry is assumed.

Implementation of electronic noise

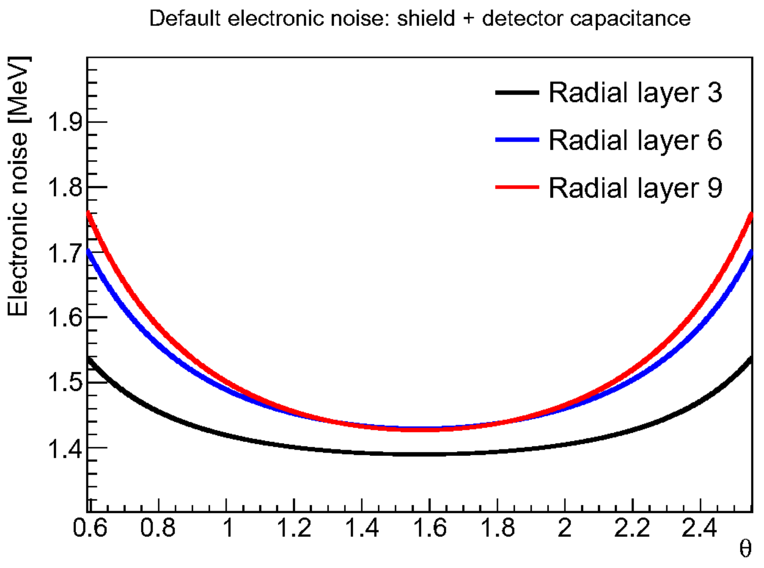

Estimation of electronic noise depending on radial layer and polar angle (unit in radian).

- The electronic noise on each ECAL cell is assumed to follow a Gaussian distribution centered at 0.
- The standard deviation of the Gaussian distribution is taken from a calculation mainly based on the size of the cell.
- During the reconstruction in the full simulation, the noise is sampled from each cell and added to its signal value.
- Noise filter: Cells with energy below a multiplier of the expected noise are removed from the output cell collection, before the cell collection is passed to clustering algorithms.

Distribution of cell signal

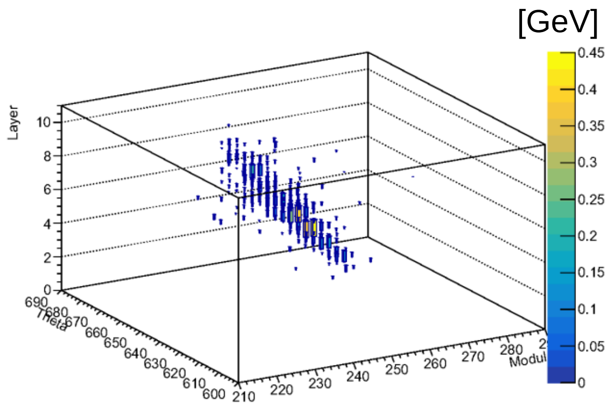

Baseline

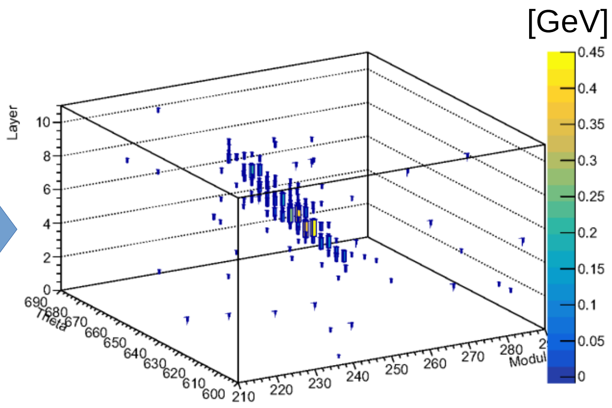

Noise (3 sigma filter)

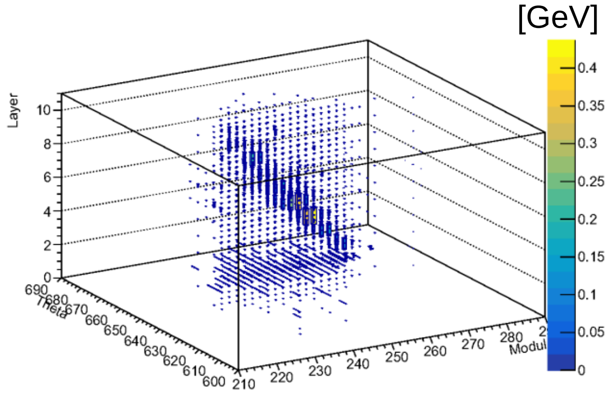

Cross-talk

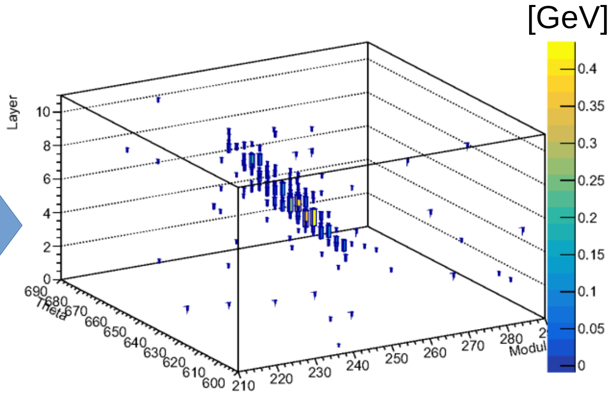

Cross-talk + noise
(3 sigma filter)

A 5 GeV photon is injected into ALLEGRO, but with different setups of cross-talk and noise.

- The cross-talk smears out the energy deposit of the photon in the ECAL.
- With the addition of electronic noise and noise filter, no visible distortion is observed for the core part of the shower.

Energy response

Noise (1 sigma filter)

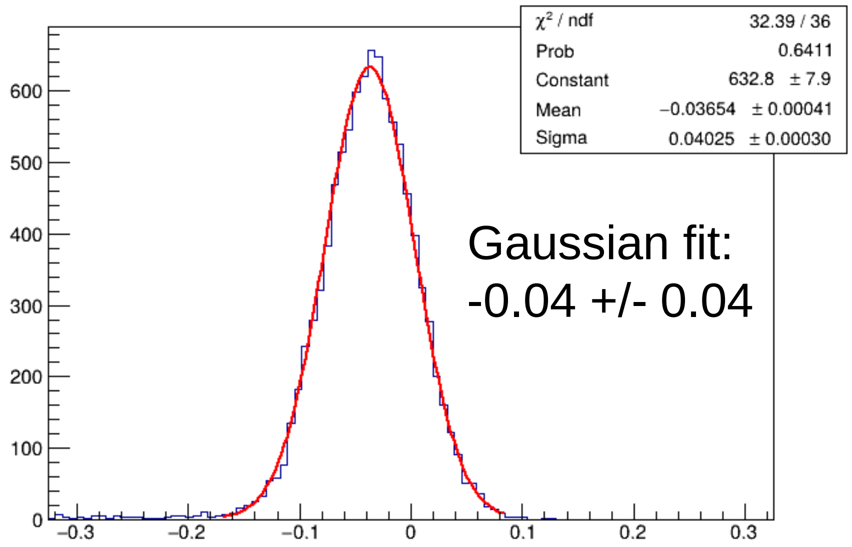

Cross-talk + noise (1 sigma filter)

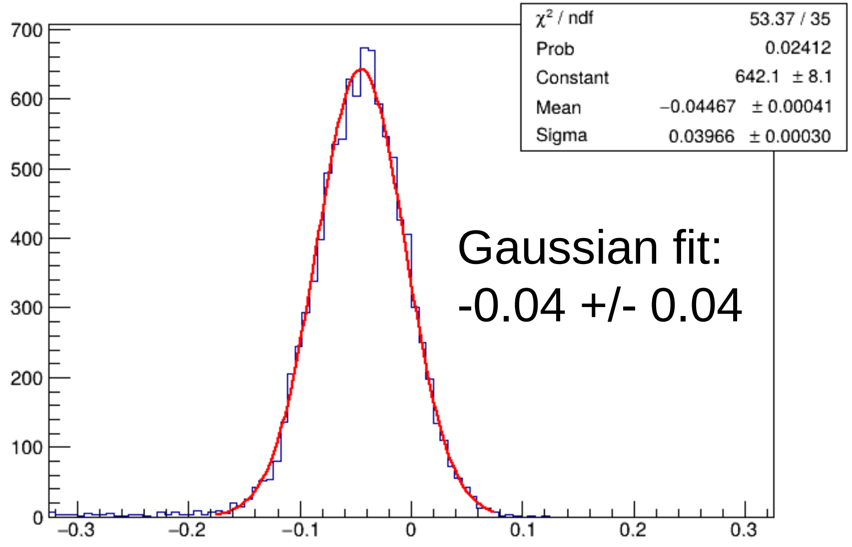

- Energy response = (E_reco – E_true) / E_true
- Distributions of energy response are studied with 10K 5 GeV photons, using CaloTopoCluster.
- The presence of cross-talk does not degrade the photon energy resolution.

ZH, H->ZZ* in 4 lepton channels at FCC-ee

A measurement of Higgs width at FCC-ee: $\Gamma_H = \frac{\sigma_{ZH}}{\sigma_{ZH,H(ZZ^*)}}\Gamma_{H\to ZZ^*}$

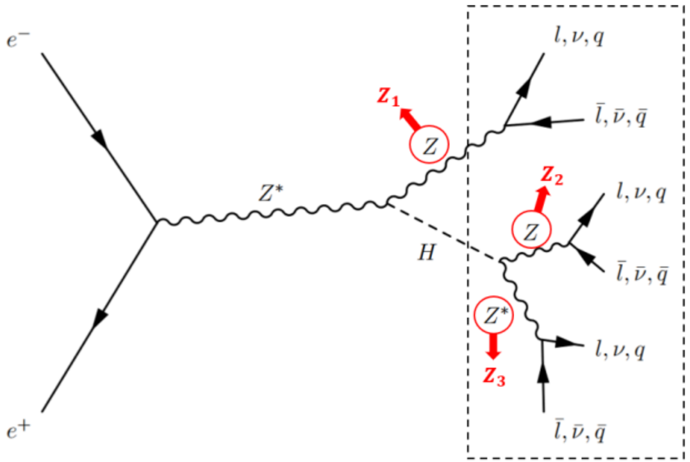

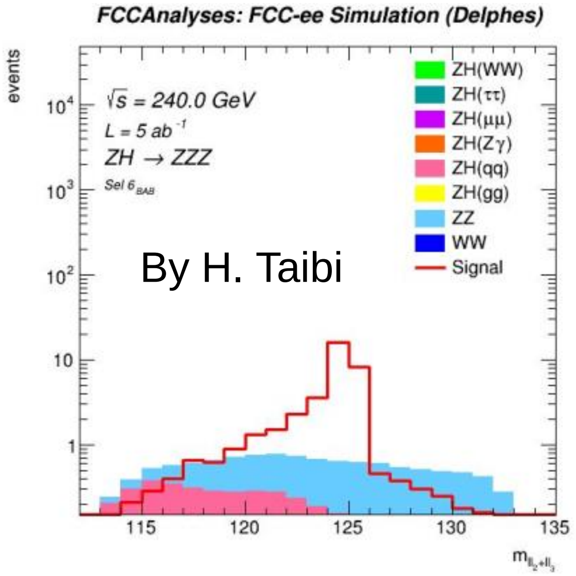

(c) Discriminating Variable of the $Z_1(jj)Z_2(ll)Z_3(ll)$ Enhanced Signature ($m_{ll_2+ll_3}$)

- Event selection: 2 lepton pairs from 2 Z-bosons. Z->vv or Z->jj for the 3rd Z-boson.
- BKG: ZZ, WW and other ZH decay channels.

The ZH, H->ZZ*->lljjvv channel has already been studied. Focusing on 4 lepton channels brings a similar sensitivity.

Choose the best discriminating variable in each channel after event selection.

ZH, H->ZZ* in 4 lepton channels at FCC-ee

- Signal strength in a template fit as POI: combination of 4 channels gives

$\mu_{\text{Asimov}} = \sigma_{\text{Asimov}}/\sigma_{\text{SM}} = 1^{+0.104}_{-0.098}$ (stat. and background cross-section uncertainties).

- Possible improvement: discriminating variables for $Z_2 \rightarrow \nu\nu$ and $Z_3 \rightarrow \nu\nu$ channels.

Channel	$S/\sqrt{B}$	Discriminating Variable
$Z_1(ll)Z_2(ll)Z_3(jj)$	$7.9 \pm \delta < 2.1$	$m^{\text{rec}}_{ll_1}$ (recoil mass of Z_1)
$Z_1(ll)Z_2(jj)Z_3(ll)$	$6.2 \pm \delta < 0.4$	m_{jj+ll_3} (mass of dijet+Z_3)
$Z_1(jj)Z_2(ll)Z_3(ll)$	$10.9 \pm \delta < 2.3$	$m_{ll_2+ll_3}$ (mass of $Z_2 + Z_3$)
$Z_1(\nu\nu)Z_2(ll)Z_3(ll)$	$2.9 \pm \delta < 0.1$	$m_{ll_2+ll_3}$ (mass of $Z_2 + Z_3$)

The 4 channels used for the fit, the corresponding signal over background ratios and discriminating variables.

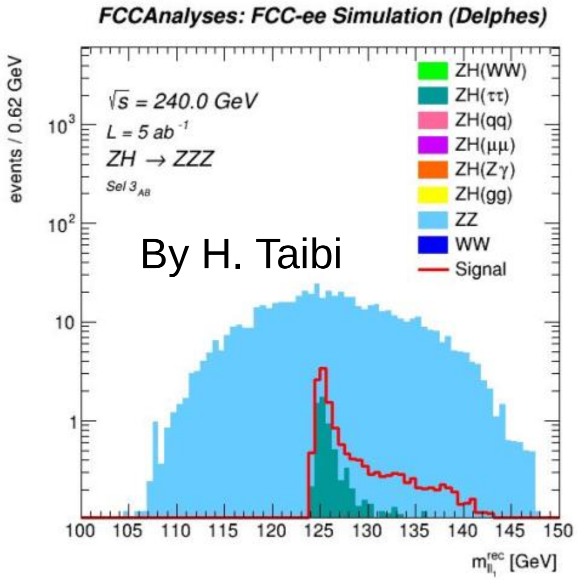

Figure 14. Distribution of the recoil mass of Z_1 for the $Z_1(ll)Z_2(ll)Z_3(\nu\nu)$ enhanced signature.

Summary

- The emulation of ECAL cross-talk has been implemented in the ALLEGRO full simulation to study the impact on physics performance.
- Electronic noise can be enabled for cells in ALLEGRO ECAL, with the function of an adjustable noise filter.
- The energy resolution of topo-cluster is stable against the presence of cross-talk. More studies are needed to investigate the impact of cross-talk on photon-pion discrimination.
- A preliminary study explores the feasibility of measuring the Higgs boson width at FCC-ee using ZH, H->ZZ* process with 4 leptons in the final state. The statistical uncertainty is estimated to be 10%, with possibility of further improvement.

Backup

The Future Circular Collider (FCC)

- The next generation collider with a circumference of ~90 km.
- Sgate 1: FCC-ee as Higgs factory, EW & top factory at highest luminosities.
- Stage 2: FCC-hh (~100 TeV): Energy frontier.

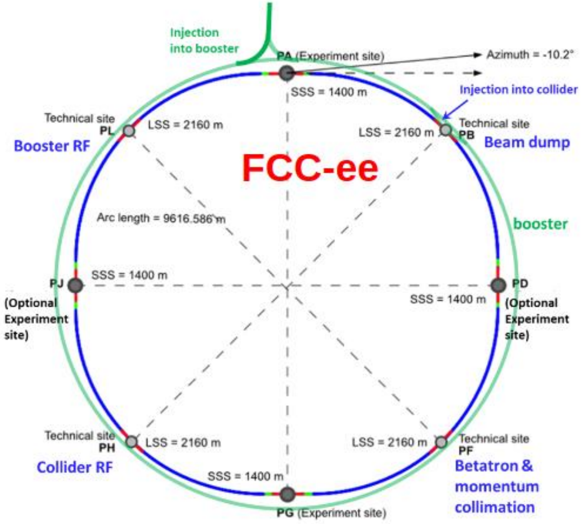

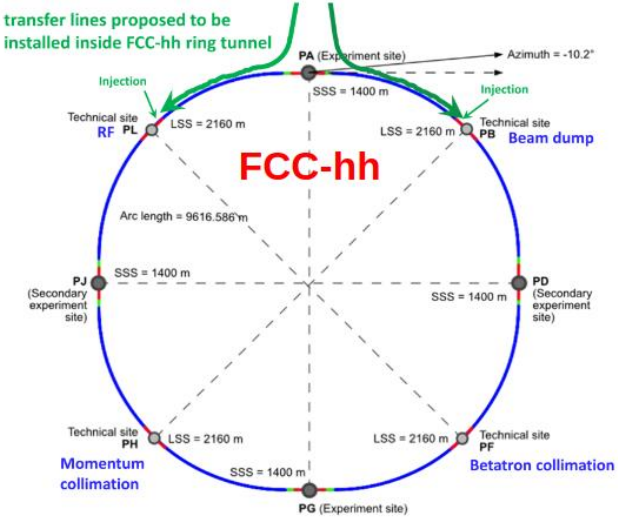

Noble liquid calorimetry

- Sampling calorimeter technology. Repeated layers of absorber, noble liquid and read-out electrode.
- EM showers start in the absorber. Electron produced in the showers ionise the liquefied noble gas and induce signals.
- Advantages: Mature technology (D0, ATLAS, …), good energy resolution, linearity, stability and uniformity, timing properties.
- Challenges: signal extraction and complex mechanical structure inside the cryostat.

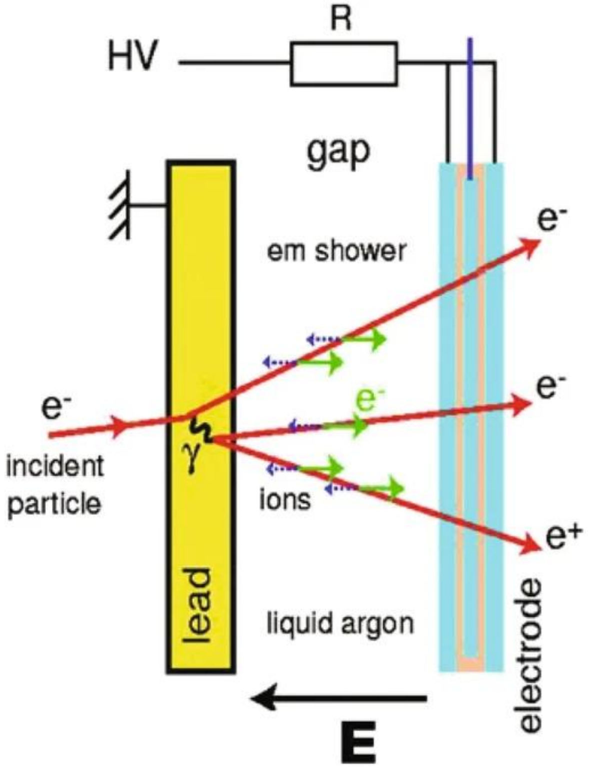

EM shower and signal induction (taken from ISBN 978-3-030-35318-6).

Read-out electrode structure

- Printed circuit board technology allows high granularity.
- Various couplings between calorimeter cells and signal traces inside the read-out electrode generate cross-talk → Need for shielding.

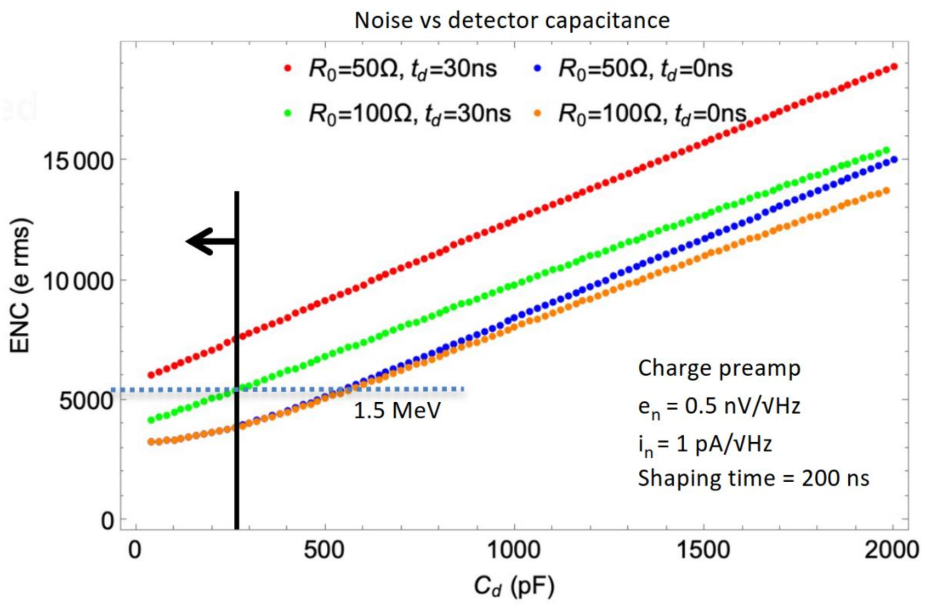

- A wider shielding reduces cross-talk but increases the detector capacitance, therefore resulting in a higher noise level.
- In the meantime, higher granularity also leads to smaller signal amplitude.

→The design of the read-out electrode is a balance among granularity, cross-talk and noise.

$$N \sim C_d \sqrt{\frac{4kT}{g_m \tau_p}}$$

Cold read-out electronics can help achieve a low-noise read-out!

Electrode prototypes

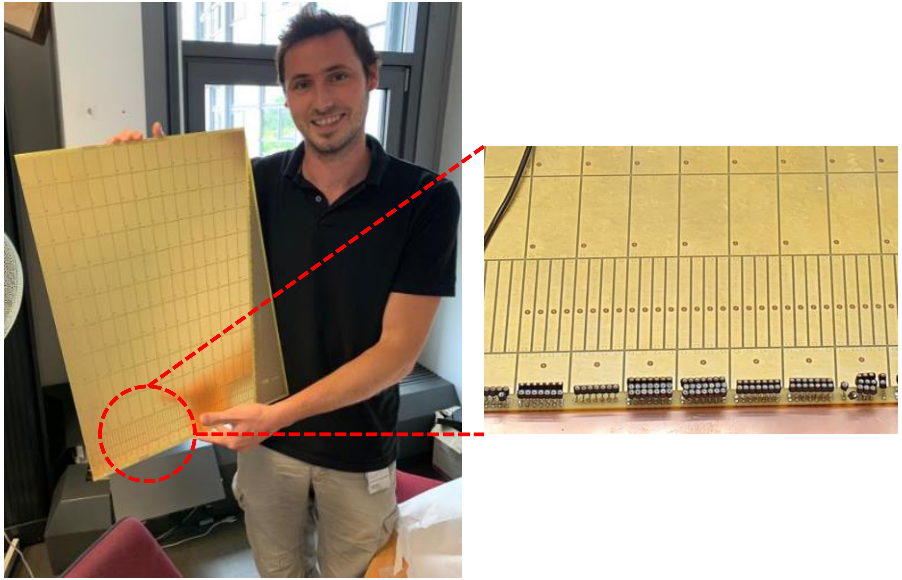

CERN prototype PCB 58 cm × 44 cm

- An inclination angle of 50 degrees → thickness = 40 cm (22 radiation length).
- Segmented into 16 θ-towers and 12 radial layers.
- 4 times higher granularity on the second layer for photon-π0 identification.

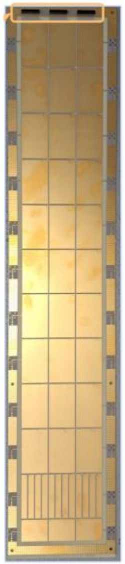

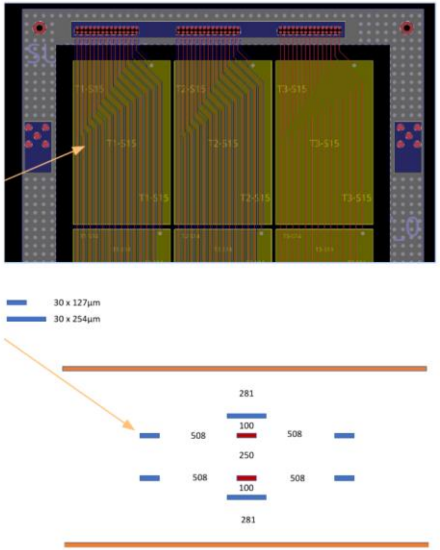

New IJCLab prototype arrived in January

- Double signal traces (which seems to increase cell capacitance significantly).
- New lateral shielding between signal traces in two of the three θ-towers, while the third one is used as reference.
- Connectors for easy signal injection and read-out. Development of automated measurements.

Simulation of read-out electrode

- Electrical properties are also studied by Ansys Electronics Desktop.
- Good agreement of cross-talk shapes between measurement and simulation.

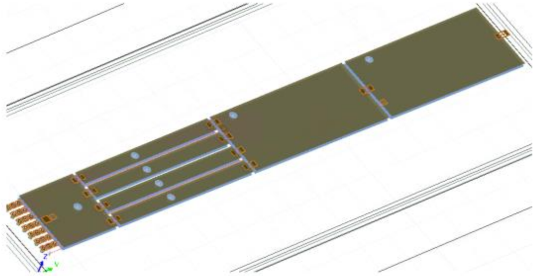

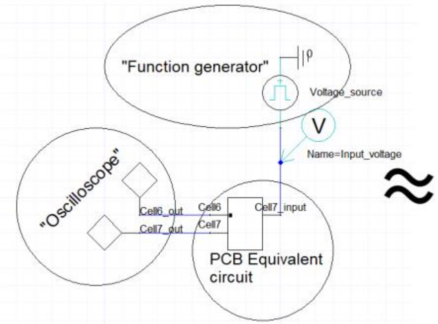

≈

PCB model analysed and converted to equivalent circuit.

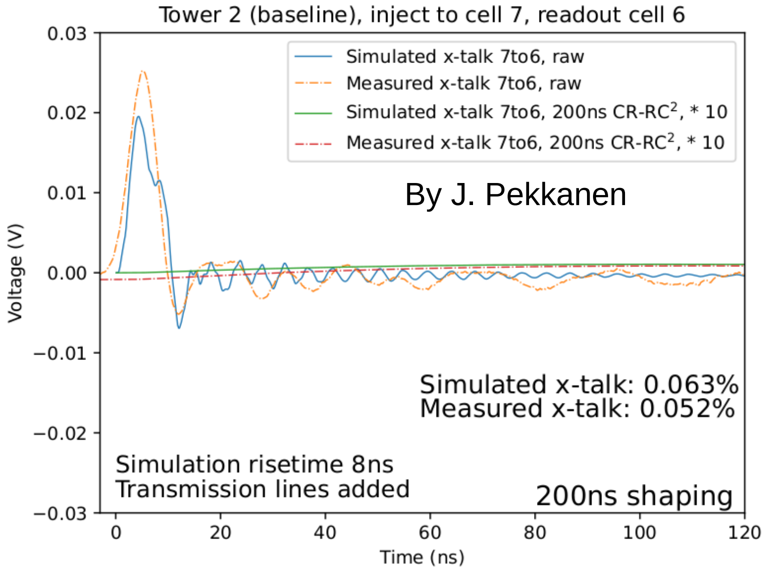

Sufficiently good reproduction of the measurement by simulation enables studies of different shielding scenarios.

ECAL endcap

The EM calorimeter in the endcap region is also a noble liquid technology sampling calorimeter.

- Requirements: high granularity (thin absorber), no dead material on the inside face, uniformity in azimuthal angle.
- One option: turbine-like geometry with ~240 repeats of absorber and read-out electrode.

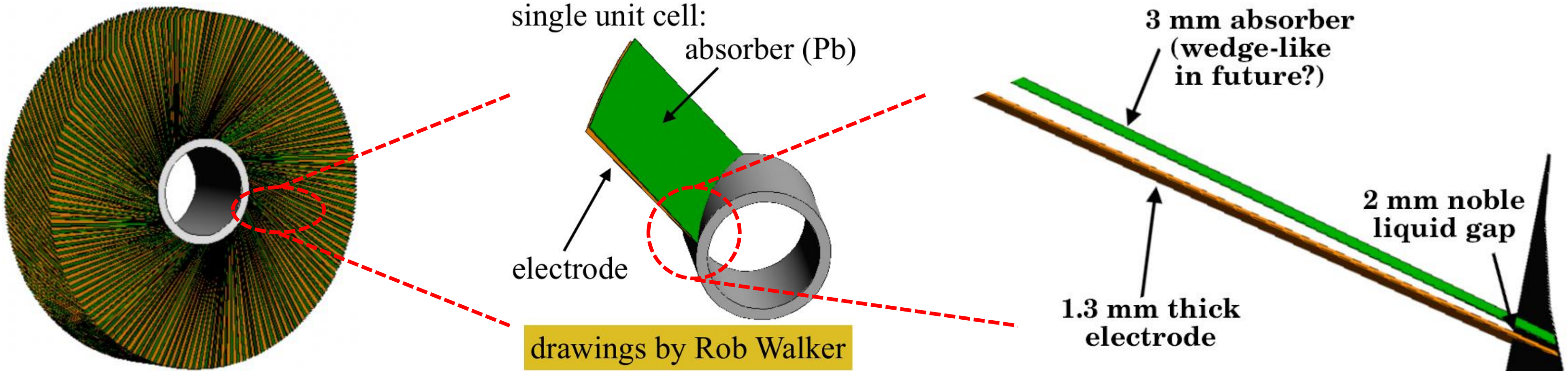

The optimisation of mechanical structure in the design is under study.

Hadronic calorimeter (HCAL)

- The design of HCAL comprises alternating layers of steel and scintillators. Also acts as the return yoke of the solenoid.
- Well studied and tested reference for the design: the ATLAS Tile Calorimeter.
- Technical parameters:

(a) 5 mm absorbers and 3 mm scintillators.

(b) 13 radially thickening layers.

(c) 128 azimuthal modules and 2 tiles per module ($\Delta\phi = 0.025$).

(d) $\Delta\eta = 0.025$ by grouping 3-4 tiles.

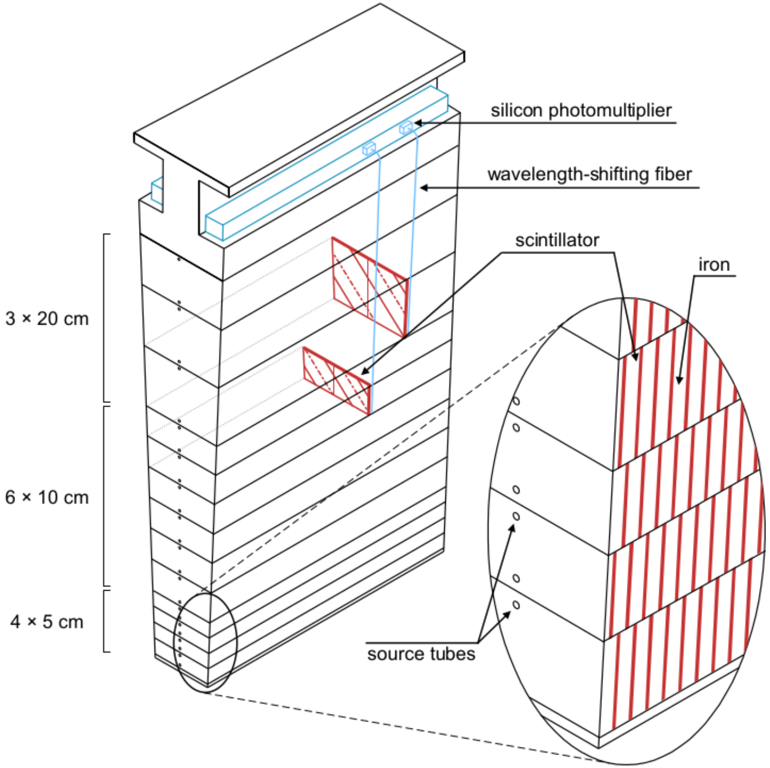

The HCAL barrel baseline geometry.

The read-out scheme

- Signals are extracted from both the inner and outer radial edges, depending on the layer.

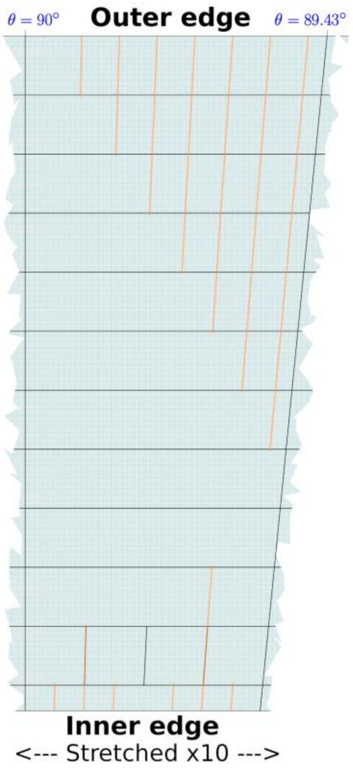

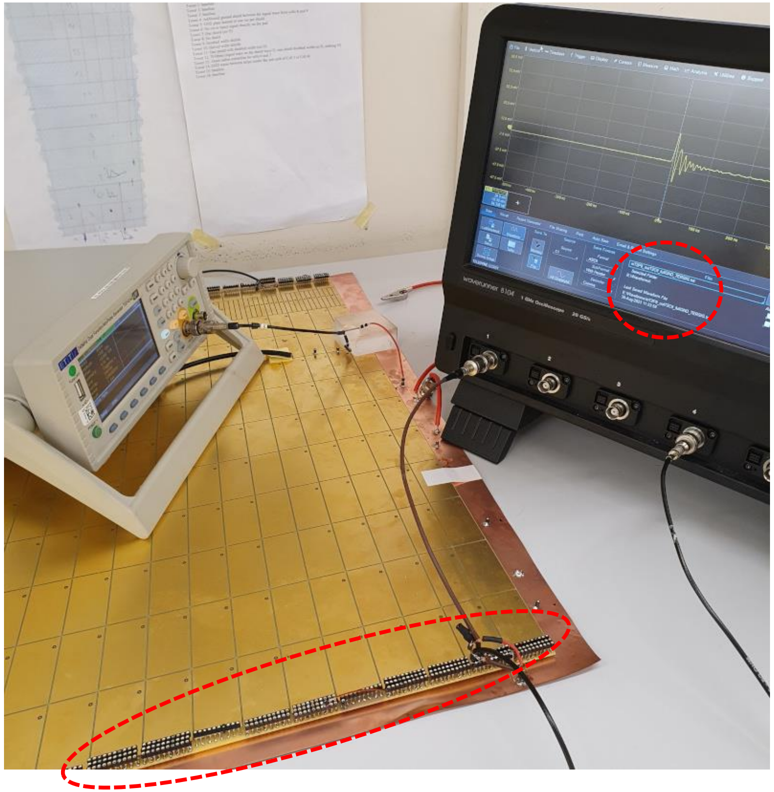

In IJCLab prototype and next CERN prototype, read-out is designed only from the outer edge in order to minimise the amount of dead material in the front.

Full simulation and cluster reconstruction

- Detector full simulation of ALLEGRO has been built to help optimise the choice of granularity and materials.
- Detector geometry definition and visualisation of the simulated event.
- ECAL+HCAL topo-cluster reconstruction has been implemented. Moving forward to the realisation of Particle Flow algorithms.

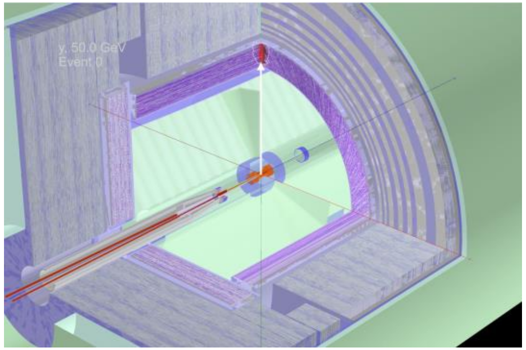

The response of the ALLEGRO caloimetry to a 50 GeV photon.

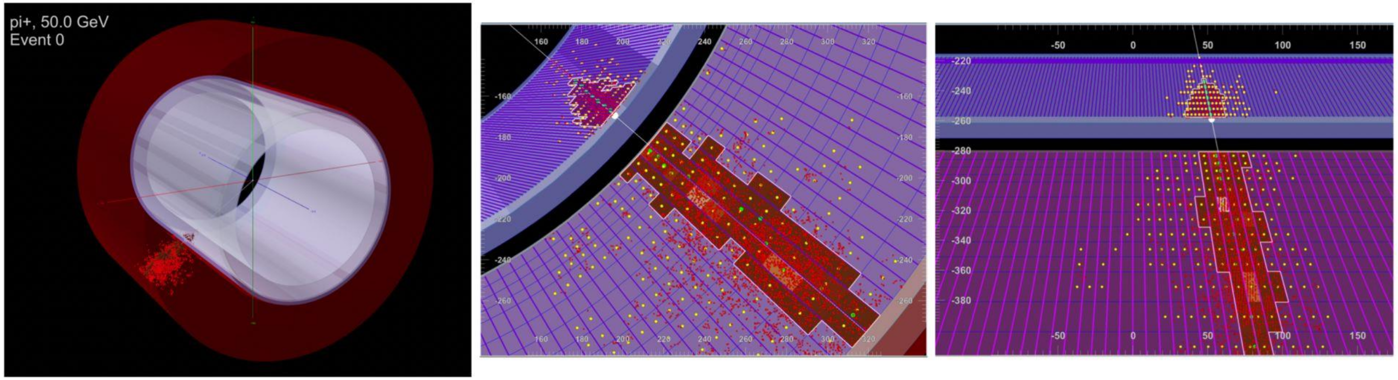

Topo-cluster reconstruction of showers generated by a 50 GeV pion in ALLEGRO calorimetry.

More details covered in Erich’s talk and in Filomena’s poster.

Expected performance

- ECAL energy resolution to single electrons has been studied for various absorber and active materials. A 7% sampling rate is achieved for the baseline Pb+LAr combination.
- Machine learning techniques are under development to provide better energy resolution for combined ECAL+HCAL cluster reconstruction.

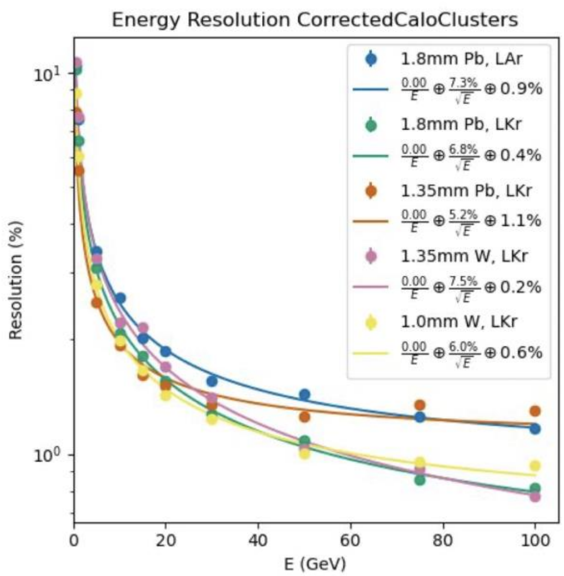

Energy resolution to single electrons for ECAL barrel.

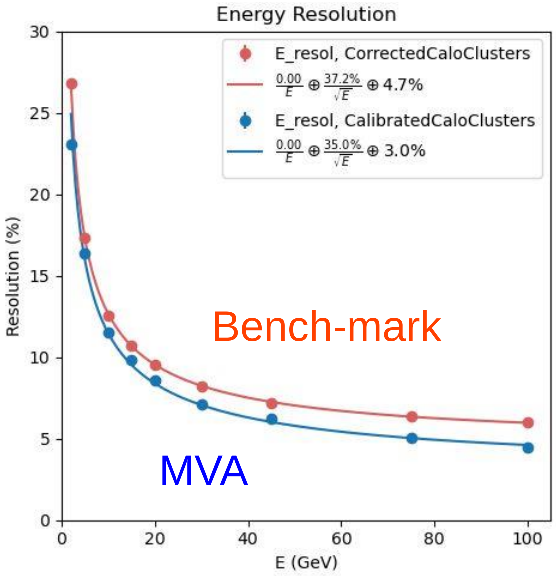

Energy resolution to single negatively-charged pions with ECAL+HCAL cluster reconstruction after different calibrations

Event selection

Variables
m_{ll_1} and m_{ll_2}: mass of the dilepton associated to Z_1 and Z_2 respectively
E^{miss}: missing energy

	Signal	Background							
Selection	$ZH(ZZ^*)$	$ZH(WW)$	$ZH(\mu\mu)$	$ZH(qq)$	$ZH(\tau\tau)$	$ZH(Z\gamma)$	$ZH(gg)$	ZZ	WW
Two $Z(ll)$ & no $Z^*(ll)$ (Sel 0_A)	113.6 ±0.5	181 ±2	7.56 ±0.01	25 ±1	59.4 ±0.6	5.76 ±0.03	0.007 ±0.007	12196 ±38	47 ±3
Sel 0_A + $m_{ll_{1,2}} \in [80, 110]$ GeV (Sel 1_A)	65.2 ±0.4	1.0 ±0.1	0.538 ±0.003	0 $\pm\delta < 1$	8.7 ±0.2	4.63 ±0.02	0 $\pm\delta < 0.007$	6286 ±28	0 $\pm\delta < 3$
Sel 1_A + $E^{\text{miss}} < 8$ GeV (Sel 2_{AA})	46.1 ±0.3	0.02 ±0.02	0.498 ±0.003	0 $\pm\delta < 1$	0.52 ±0.05	4.34 ±0.02	0 $\pm\delta < 0.007$	4817 ±24	0 $\pm\delta < 3$
Sel 1_A + $E^{\text{miss}} > 8$ GeV (Sel 2_{AB})	19.1 ±0.2	1.0 ±0.1	0.0399 ±0.0009	0 $\pm\delta < 1$	8.2 ±0.2	0.289 ±0.006	0 $\pm\delta < 0.007$	1468 ±13	0 $\pm\delta < 3$

Table 3. Cutflow of the $Z_1(ll)Z_2(ll)Z_3(xx)$ channels.

Event selection

Variables
m_{ll}: mass of the dilepton associated to the on-shell Z (Z_1 or Z_2)
m_{ll_3}: mass of the dilepton associated to the off-shell Z (Z_3)
E^{miss}: missing energy

	Signal	Background							
Selection	$ZH(ZZ^*)$	$ZH(WW)$	$ZH(\mu\mu)$	$ZH(qq)$	$ZH(\tau\tau)$	$ZH(Z\gamma)$	$ZH(gg)$	ZZ	WW
One $Z(ll)$ & one $Z^*(ll)$ (Sel 0_B)	206.8 ± 0.8	270 ± 2	5.97 ± 0.01	951 ± 7	130.5 ± 0.8	1.17 ± 0.01	5.1 ± 0.2	28340 ± 59	846 ± 14
Sel 0_B + $m_{ll} \in [80, 110]$ GeV (Sel 1_B)	173.4 ± 0.7	246 ± 2	5.27 ± 0.01	866 ± 6	118.6 ± 0.8	1.06 ± 0.01	4.7 ± 0.2	15680 ± 44	257 ± 8
Sel 1_B + $m_{ll_3} \in [10, 40]$ GeV (Sel 2_B)	158.2 ± 0.7	187 ± 2	0.0288 ± 0.0007	462 ± 4	76.4 ± 0.6	0.337 ± 0.007	0.77 ± 0.07	3097 ± 19	12 ± 2
Sel 2_B + $E^{\text{miss}} < 8$ GeV (Sel 3_{BA})	96.4 ± 0.5	1.4 ± 0.2	0.0268 ± 0.0007	155 ± 2	0.19 ± 0.03	0.152 ± 0.005	0.32 ± 0.05	1412 ± 13	0 $\pm\delta < 2$
Sel 2_B + $E^{\text{miss}} > 8$ GeV (Sel 3_{BB})	61.8 ± 0.4	186 ± 2	0.0020 ± 0.0002	307 ± 4	76.2 ± 0.6	0.185 ± 0.005	0.45 ± 0.06	1685 ± 14	12 ± 2

Table 4. First selections on the $Z_1(ll)Z_2(xx)Z_3(ll)$ and $Z_1(xx)Z_2(ll)Z_3(ll)$ channels.

Event selection

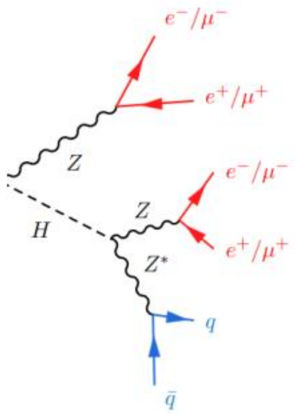

Figure 7. $llljj$ decay.

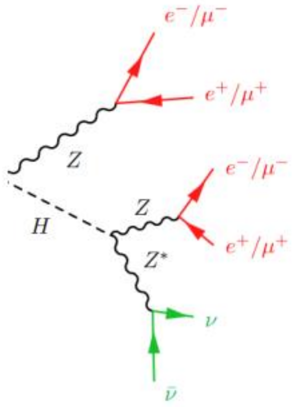

Figure 8. $llll\nu\nu$ decay.

Variables
E^γ: energy of the highest-energy photon $m^{\text{rec}}_{ll_2+\gamma}$: recoil mass of the four-vector obtained by the summing the Z_2 four-vector and the highest-energy photon four-vector

	Signal	Background							
Selection	$ZH(ZZ^*)$	$ZH(WW)$	$ZH(\mu\mu)$	$ZH(qq)$	$ZH(\tau\tau)$	$ZH(Z\gamma)$	$ZH(gg)$	$\boldsymbol{ZZ}$	WW
Sel 2_{AA} + $E^\gamma < 20$ GeV (Sel 3_{AA})	45.1 ±0.3	0.02 ±0.02	0.204 ±0.002	0 $\pm < 1$	0.43 ±0.05	0.135 ±0.004	0 $\pm\delta < 0.007$	3539 ±21	0 $\delta < 3$
Sel 3_{AA} + $m^{\text{rec}}_{ll_2+\gamma} > 115$ GeV (Sel 4_{AA})	41.3 ±0.3	0.02 ±0.02	0.0160 ±0.0005	0 $\pm\delta < 1$	0.32 ±0.04	0.030 ±0.002	0 $\pm\delta < 0.007$	29 ±2	0 $\pm\delta < 3$

Table 5. Cutflow of the $Z_1(ll)Z_2(ll)Z_3(jj)$ channel.

Variables
$m^{\text{rec}}_{ll_2}$: recoil mass of the dilepton associated to Z_2

	Signal	Background							
Selection	$ZH(ZZ^*)$	$ZH(WW)$	$ZH(\mu\mu)$	$ZH(qq)$	$\boldsymbol{ZH(\tau\tau)}$	$ZH(Z\gamma)$	$ZH(gg)$	$\boldsymbol{ZZ}$	WW
Sel 2_{AB} + $m^{\text{rec}}_{ll_2} \in [125, 150]$ GeV (Sel 3_{AB})	16.1 ±0.2	0.7 ±0.1	0.0267 ±0.0007	0 $\pm\delta < 1$	6.8 ±0.2	0.264 ±0.006	0 $\pm\delta < 0.007$	577 ±8	0 $\pm\delta < 3$

Table 6. Cutflow of the $Z_1(ll)Z_2(ll)Z_3(\nu\nu)$ channel.

Event selection

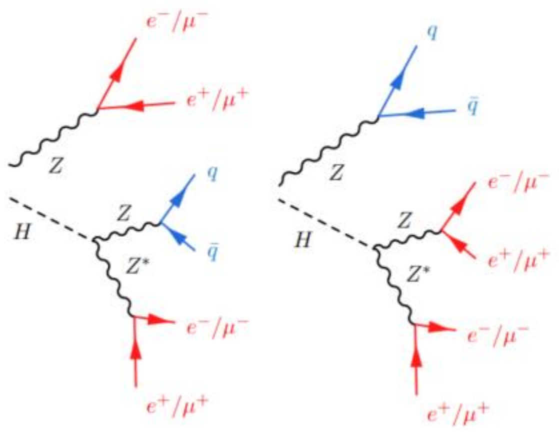

Figure 9. $lljjll$ decay (left) and $jjllll$ decay (right).

Variables

m_{jj}: mass of the dijet
$m^{\text{rec}}_{ll_3}$: recoil mass of the dilepton associated to Z_3
$m^{\text{rec}}_{jj+ll_3}$: recoil mass of the four-vector obtained by summing the dijet four-vector and the Z_3 four-vector

	Signal	Background							
Selection	$ZH(ZZ^*)$	$ZH(WW)$	$ZH(\mu\mu)$	$\boldsymbol{ZH(qq)}$	$ZH(\tau\tau)$	$ZH(Z\gamma)$	$ZH(gg)$	$\boldsymbol{ZZ}$	WW
Sel 3_{BA} + $\Delta > 0$ (Sel 4_{BAA})	51.5 ±0.4	1.3 ±0.2	0.0248 ±0.0007	137 ±2	0.19 ±0.03	0.127 ±0.004	0.21 ±0.04	741 ±9	0 $\pm\delta < 2$
Sel 4_{BAA} + $m_{jj} \in [80, 110]$ GeV (Sel 5_{BAA})	44.8 ±0.3	0.30 ±0.07	0.0005 ±0.0001	101 ±2	0.011 ±0.008	0.064 ±0.003	0.20 ±0.04	23 ±2	0 $\pm\delta < 2$
Sel 5_{BAA} + $m^{\text{rec}}_{ll_3} \in [190, 215]$ GeV (Sel 6_{BAA})	40.6 ±0.3	0.07 ±0.04	0.0005 ±0.0001	40 ±1	0.005 ±0.005	0.024 ±0.002	0.04 ±0.02	10 ±1	0 $\pm\delta < 2$
Sel 6_{BAA} + $m^{\text{rec}}_{jj+ll_3} \in [80, 110]$ GeV (Sel 7_{BAA})	40.1 ±0.3	0.07 ±0.03	0.0005 ±0.0001	34 ±1	0.005 ±0.005	0.022 ±0.002	0.04 ±0.02	8 ±1	0 $\pm\delta < 2$

Table 7. Cutflow of the $Z_1(ll)Z_2(jj)Z_3(ll)$ channel.

Variables

m_{jj}: mass of the dijet
$m^{\text{rec}}_{ll_3}$: recoil mass of the dilepton associated to Z_3
$m_{ll_2+ll_3}$: mass of the four-vector obtained by summing the Z_2 four-vector and the Z_3 four-vector

	Signal	Background							
Selection	$ZH(ZZ^*)$	$ZH(WW)$	$ZH(\mu\mu)$	$\boldsymbol{ZH(qq)}$	$ZH(\tau\tau)$	$ZH(Z\gamma)$	$ZH(gg)$	$\boldsymbol{ZZ}$	WW
Sel 3_{BA} + $\Delta < 0$ (Sel 4_{BAB})	44.9 ±0.4	0.11 ±0.05	0.0020 ±0.0002	18.3 ±0.8	0 $\pm\delta < 0.03$	0.024 ±0.002	0.11 ±0.03	663 ±9	0 $\pm\delta < 2$
Sel 4_{BAB} + $m_{jj} \in [80, 110]$ GeV (Sel 5_{BAB})	42.4 ±0.4	0.11 ±0.05	$2.8\ 10^{-4}$ $\pm0.8\ 10^{-4}$	16.0 ±0.8	0 $\pm\delta < 0.03$	0.017 ±0.002	0.09 ±0.03	87 ±3	0 $\pm\delta < 2$
Sel 5_{BAB} + $m^{\text{rec}}_{ll_3} \in [195, 215]$ GeV (Sel 6_{BAB})	38.3 ±0.4	0.02 ±0.02	$1.2\ 10^{-4}$ $\pm0.5\ 10^{-4}$	4.4 ±0.4	0 $\pm\delta < 0.03$	0.006 ±0.001	0.02 ±0.01	9 ±1	0 $\pm\delta < 2$

Table 8. Cutflow of the $Z_1(jj)Z_2(ll)Z_3(ll)$ channel.

Event selection

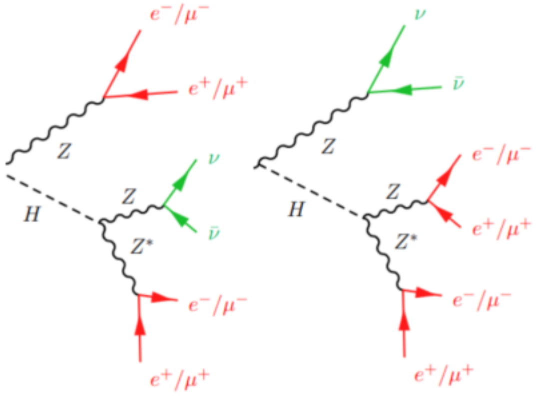

Figure 10. $ll\nu\nu ll$ decay (left) and $\nu\nu llll$ decay (right).

Variables
m_{ll}^{rec}: recoil mass of the dilepton associated to the on-shell Z (Z_1 or Z_2).

	Signal	Background							
Selection	$ZH(ZZ^*)$	$\boldsymbol{ZH(WW)}$	$ZH(\mu\mu)$	$\boldsymbol{ZH(qq)}$	$\boldsymbol{ZH(\tau\tau)}$	$ZH(Z\gamma)$	$ZH(gg)$	$\boldsymbol{ZZ}$	$\boldsymbol{WW}$
Sel 3_{BB} + $m_{ll}^{\text{rec}} \in [123, 127]$ GeV (Sel 4_{BBA})	20.3 ±0.42	119 ±1	2 10^{-5} ±2 10^{-5}	195 ±3	49.0 ±0.5	0.114 ±0.004	0.29 ±0.05	84 ±3	1.1 ±0.5

Table 9. Cutflow of the $Z_1(ll)Z_2(\nu\nu)Z_3(ll)$ channel.

Variables
m_{ll}^{rec}: recoil mass of the dilepton associated to the on-shell Z (Z_1 or Z_2)
E^{miss}: missing energy
m^{vis}: visible mass

	Signal	Background							
Selection	$ZH(ZZ^*)$	$\boldsymbol{ZH(WW)}$	$ZH(\mu\mu)$	$ZH(qq)$	$\boldsymbol{ZH(\tau\tau)}$	$ZH(Z\gamma)$	$ZH(gg)$	$\boldsymbol{ZZ}$	WW
Sel 3_{BB} + $m_{ll}^{\text{rec}} \notin [123, 127]$ GeV (Sel 4_{BBB})	38.1 ±0.4	67 ±1	0.0020 ±0.0002	112 ±2	27.2 ±0.4	0.070 ±0.003	0.16 ±0.03	1601 ±14	11 ±2
Sel 4_{BBB} + $E^{\text{miss}} \in [45, 55]$ GeV (Sel 5_{BBB})	12.3 ±0.2	12.9 ±0.5	0 $\pm\delta < 0.0002$	0.4 ±0.1	4.5 ±0.2	0.0040 ±0.0007	0 $\pm\delta < 0.03$	161 ±4	2.0 ±0.7
Sel 5_{BBB} + $m^{\text{vis}} < 135$ GeV (Sel 6_{BBB})	12.0 ±0.2	2.0 ±0.2	0 $\pm\delta < 0.0002$	0 $\pm\delta < 0.1$	3.1 ±0.1	0.0002 ±0.0001	0 $\pm\delta < 0.03$	13 ±1	0.7 ±0.4

Table 10. Cutflow of the $Z_1(\nu\nu)Z_2(ll)Z_3(ll)$ channel.

Discriminating variable in the llllјj channel

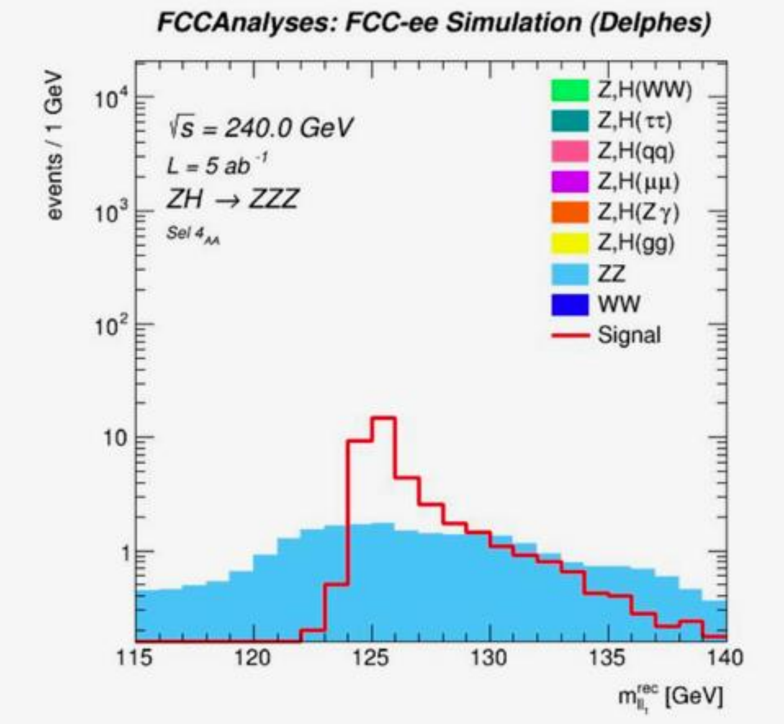

(a) Discriminating Variable of the $Z_1(ll)Z_2(ll)Z_3(jj)$ Enhanced Signature ($m_{ll_1}^{\mathrm{rec}}$)